Propagating plasmonic mode in nanoscale apertures and its implications for extraordinary transmission

Peter B. Catrysse and Shanhui Fan
Edward L. Ginzton Laboratory and Department of Electrical Engineering
Stanford University, Stanford, CA 94305-4088
pcatryss@stanford.edu

Abstract: We studied the interaction of different pathways by which extraordinary transmission through nanoscale aperture arrays arises and obtained a complete physical picture that incorporates both propagating plasmonic and surface plasmon modes. The transmission behavior is qualitatively different depending on the number of transmission pathways present in the regime of operation. If only one pathway is present, it can give rise to high transmission. When multiple pathways are present simultaneously, their interplay must be studied in order to understand the rich and complex transmission behavior. The frequency range of these pathways can be controlled by varying the structures and, in particular, by coating the surface of the arrays or by filling the apertures with dielectrics that differ from the surrounding medium.

Keywords: apertures, aperture arrays, extraordinary transmission, Fano interference, nano-scale apertures, plasmon-polaritonic material, propagating plasmonic modes, surface plasmon modes, transmission pathways, transmission suppression

1 INTRODUCTION

The optical properties of nanoscale apertures in optically thick metallic films have been intensely researched in the past several years due to their fundamental importance in near-field optics and nano-photonics, as well as their practical significance for photonic devices and applications, including filters, near-field probes, optical data storage, and nano-lithography [1,2]. It is well-established that the transmission characteristics of apertures strongly vary depending on whether they allow or prohibit propagating modes [3,4]. For example, enhanced transmission in metallic nano-slits is attributed to propagating transverse magnetic (TM) modes that are supported by slits, *independent of their width* [3,5-9]. Cylindrical holes with a circular cross-section in a perfect metal, on the other hand, do not support propagating modes when the hole diameter is smaller than $\lambda/2n_0$, where λ is the vacuum wavelength of incident light and n_0 is the refractive index of the dielectric inside the hole [10,11]. Following Ebbesen *et al.*'s pioneering experiments [12], extraordinary optical transmission has therefore commonly been associated with the excitation of surface wave resonances on the front and back surfaces of the metallic film and an evanescent tunneling process through the subwavelength holes [11-16]. More recently, localized surface plasmon modes or shape resonances inside subwavelength holes have been identified as an alternative pathway for extraordinary transmission [17-22]. In either case, the use of resonances results in transmission peaks of relatively narrow line width. In recent work of our own, we numerically demonstrated that subwavelength holes in a metal always support a propagating plasmonic HE_{11} mode near the surface plasmon frequency, *regardless of how small the holes are*, and that this mode can lead to near-complete optical transmission through a subwavelength hole array [23,24]. The importance of such propagating modes is that, under appropriate conditions, they provide a transmission window with a relatively broad bandwidth. Hence, it has become clear that there are multiple mechanisms by which

Received 4 Sep 2007; accepted 20 Dec 2007; published 12 Feb 2008 [CCC: 19342608/2008/$25.00]

extraordinary transmission can occur. The interaction between these mechanisms, however, has not received much attention.

In this paper, we study the interference of different mechanisms or pathways by which extraordinary transmission through subwavelength hole arrays arises. We provide a complete physical picture that incorporates all previously reported pathways and unifies them in a comprehensive framework based on the analysis of their respective dispersion relations. We show that the transmission behavior is qualitatively different depending on the number of transmission pathways present in the regime of operation. If only one mechanism is present, it gives rise to extraordinary transmission. When multiple mechanisms are present simultaneously, their interplay must be studied in order to understand the rich and complex transmission behavior. We further demonstrate that the frequency range of these pathways can be controlled by varying the structures and, in particular, by coating the surface of the hole arrays or by filling the holes with dielectrics that differ from the surrounding medium.

This paper is organized as follows: we start by revisiting the regime explored in experiments inspired by Ebbesen *et al.* and we show that our approach explains all the salient features in the transmission spectrum, including the ones ascribed to surface waves. In addition, we provide evidence that shape resonances or localized surface plasmons are, in fact, due to the behavior near cut-off of propagating plasmonic modes inside the holes. Next, we design subwavelength hole arrays that probe other regimes of operation in which either one or multiple pathways are present. In each case, a dispersion analysis explains all the details of the transmission spectrum.

2 BACKGROUND AND NUMERICAL APPROACH

Following Ebbesen *et al.*'s pioneering experiments [12], the most-studied pathway for extra-ordinary optical transmission through subwavelength hole arrays has been surface waves. As a starting point, we analyze the transmission properties of a subwavelength hole array with a 750-nm period (a) square lattice in a 320-nm thick (h) metallic film (Fig. 1 inset). This structure was previously investigated experimentally and analyzed theoretically by Martin-Moreno *et al.* [14]. In our analysis, for simplicity and without loss of generality, we assume cylindrical holes with a circular cross-section and a 120-nm radius (r_0).

We describe the optical properties of the metal using a Drude free-electron or plasmonic model:

$$\varepsilon_1(\omega) = 1 - \frac{\omega_p^2}{\omega(\omega - i\omega_\tau)}, \tag{1}$$

where ω represents (angular) frequency, ω_p is the plasma frequency and ω_τ is the collision frequency. The dielectric function in this model takes into account the contribution of free electrons only and displays a plasma-like dispersion. Despite its apparent simplicity, the plasmonic model has been a valuable source of insights into the behavior of real metals. Its regime of validity extends deep into the visible wavelength regime for aluminum and most alkali metals [25]. It has proven to be accurate in the near- and far-infrared wavelength regimes in describing the optical behavior of noble metals (e.g., silver, gold, copper) [26,27], while being a reasonable approximation in the visible wavelength range above 500 nm. In this paper, for example, we model silver with parameter values $\omega_p = 1.37\times10^{16}$ rad/s and $\omega_\tau = 7.29\times10^{13}$ rad/s. By allowing for additional Lorentzian resonance terms, the use of the plasmonic model can be easily extended to the entire visible wavelength range, i.e., below 500 nm, where inter-band transitions often contribute to the dielectric function [28]. While a model extension of this type might be more realistic and result in applicability to a larger group of metals in a wider wavelength range, its study is beyond the scope of this paper.

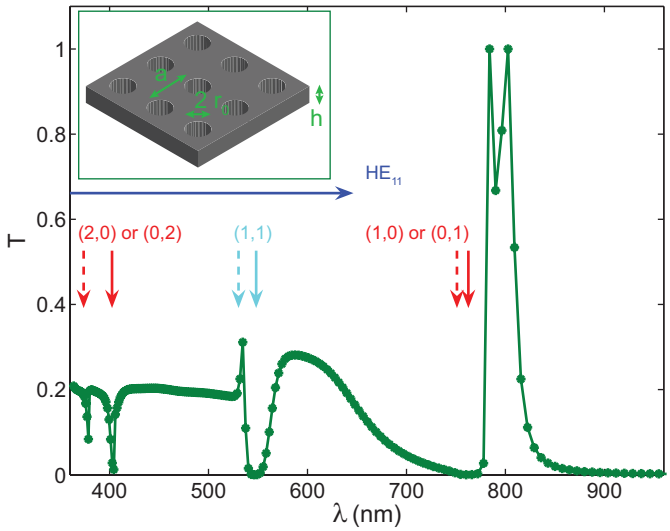

Fig. 1. Normal-incidence transmission spectrum of a cylindrical hole array with 120-nm radius (r_0) holes on a 750-nm period (a) square lattice in a 320-nm (h) thick metallic film surrounded by air. The inset shows the geometry. The surface plasmon-polariton resonances are indicated by solid red and cyan vertical arrows and the corresponding Rayleigh-Wood anomalies by dashed vertical arrows of the same color. The blue horizontal arrow shows the range of the propagating plasmonic HE_{11} mode in the hole.

For the transmission calculations, we use a three-dimensional (3D) total-field finite-difference time-domain (FDTD) implementation [29]. The simulation domain includes a single unit cell of the square-lattice array. On the top and bottom surfaces of the computational domain, we impose Perfectly Matched Layer (PML) absorbing boundary conditions [30]. For the remaining four surfaces that are perpendicular to the metallic film, we impose Bloch periodic boundary conditions [31]. Furthermore, we apply a normally incident pulsed plane-wave excitation to obtain the response in the visible and near-infrared wavelength range from a single simulation. The incidence plane is chosen above the metallic film and the field data for determining the spectral transport properties of the waveguide, through direct integration of the Poynting vector, are collected in an observation plane placed behind the metallic film. Such calculation measures the total amount of power that can pass through the hole array. The transmittance is defined as the ratio of the power passing through the subwavelength hole array to the incident power.

Figure 1 shows the calculated transmission spectrum at normal incidence for the aforementioned structure. The spectrum agrees very well with published experimental transmission measurements (Fig. 1 in Ref. 14). Moreover, it matches almost perfectly with reported theoretical transmission calculations for a structure with 240-nm wide square holes (Figs. 2 and 3 in Ref 14). In that paper, the authors provided the first three-dimensional theoretical study of extraordinary transmission through subwavelength hole arrays and showed close correspondence between their numerical results and experiments. They also developed a simplified analytic model to account for the longest-wavelength feature. In their analytic model, they attribute the highest peaks in the spectrum at 800 nm to the excitation of a surface wave resonance on the top and bottom metal-dielectric interfaces and the twin peaks to the formation of an "SP molecule" [14]. Their model, however, does not account for the remaining features in the transmission spectrum. In what follows, we show that a description

based on surface plasmon-polariton resonances alone, in fact, does not capture the full physics involved in the transport properties of light through subwavelength hole arrays. To support our claims, we provide an analysis based on dispersion for all the modes supported by the structure. We show that our model indeed captures all the physics of light transport through subwavelength hole arrays and that it quantitatively explains all the features in the transmission spectrum, including those that can not be explained by surface plasmon-polariton modes alone.

3 DISPERSION ANALYSIS

We seek to understand the properties of extraordinary transmission, by performing a dispersion analysis of the surface waves on the flat metal-dielectric interfaces, and the propagating modes inside the subwavelength holes. Both the interfaces and the holes are integral components in systems that feature extraordinary transmission. When the metal is assumed to exhibit a plasmonic response [Eq. (1)], neither of these components is inert; rather, each component plays an active and distinctive role in the transmission behavior.

3.1 Surface waves on flat metal-dielectric interfaces

A flat interface between a dielectric, with a positive dielectric function $\varepsilon_2 > 0$, and a metal, for which the real part of the dielectric function $\varepsilon_1(\omega)$ is negative, supports surface waves provided that $|\varepsilon_1(\omega)| > \varepsilon_2$ (Fig. 2 inset). Such surface plasmon-polaritons (SPPs) have wavevectors $k_{SPP}(\omega)$ related to the wave frequency ω by the following dispersion relation,

$$k_{SPP}(\omega) = \frac{\omega}{c}\sqrt{\frac{\varepsilon_1(\omega)\varepsilon_2}{\varepsilon_1(\omega)+\varepsilon_2}}\,. \tag{2}$$

Figure 2 shows the dispersion relation for surface plasmon-polaritons on a single flat metal-dielectric interface (solid blue curve). While it covers the entire frequency range from zero to the surface plasmon frequency $\omega_{sp} = \omega_p / \sqrt{1+\varepsilon_2}$, we identify two regimes with qualitatively different properties. At small frequencies, the SPP dispersion relation lies below the light line in the dielectric (dashed gray curve), but does not substantially deviate from it. This is the "photon" regime, in which the excited surface waves are highly delocalized and their fields extend far away from the metal film. The SPP wave extends significantly into the dielectric and the field concentration is largely diminished. At frequencies closer to the surface plasmon frequency, the dispersion relation lies far to the right of the light line in the dielectric and the SPPs become deep-subwavelength. We call this the "plasmon" regime, where the surface waves are very localized and their fields are highly concentrated near the interface.

In general, SPPs on a flat metal-dielectric interface are confined to the surface; they can not couple to far-field incident light. The presence of a periodic array, however, provides a phase-matching mechanism that allows surface waves to couple to normally incident light. The frequencies ω_{mn} at which surface waves are resonantly excited by a square lattice of period a are estimated using

$$\left|k_{SPP}(\omega_{mn})\right| = \sqrt{m^2+n^2}\,\frac{2\pi}{a}\,, \tag{3}$$

where m, n are integers [12]. The use of such surface resonances to enhance transmission is well documented. In past studies, the lowest-order surface wave resonance (1,0) or (0,1), which usually provides the strongest signature, has received most attention [14].

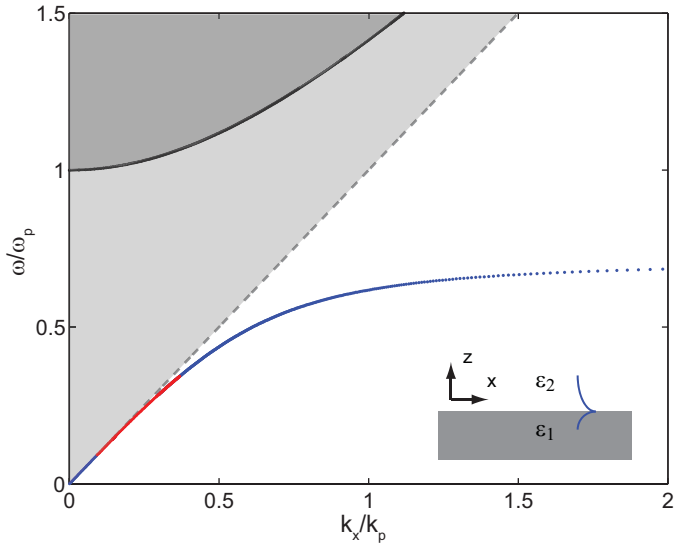

Fig. 2. Dispersion relation for surface plasmon-polaritons (SPPs) on a single flat metal-dielectric interface (blue curve). The inset shows the geometry. The red curve indicates the regimes of extraordinary transmission probed in experiments inspired by Ebbesen *et al.* The black curve depicts the bulk metal dispersive properties. Shaded areas represent the continuum of modes extended in the respective materials. Dashed gray line represents the light line in the dielectric (air).

In such a case, the surface resonance is in the "photon" regime, where the surface plasmon-polariton exhibits low losses (solid red curve). Meanwhile, higher-order modes also show up as distinct features in the transmission spectrum. As can be seen from Eq. (3), the transmission properties for any periodic structure that relies on this pathway will be highly dependent on the lattice constant a of the array (and the dielectric constant of the material interfacing with the metal). Conversely, the lattice constant a is an important design parameter for any extraordinary transmission based on this mechanism.

3.2 Propagating modes inside subwavelength holes

The propagating modes inside a subwavelength hole are calculated by considering a z-invariant cylindrical waveguide with a circular cross-section of radius r_0 in the transverse xy-plane (Fig. 3 inset). For the dielectric inside the hole, we use a real, frequency-independent dielectric function ε_3. For the surrounding metal, we assume a frequency-dependent dielectric function $\varepsilon_1(\omega)$. The propagating modes (m,n) of the waveguide are found by solving Maxwell's equations in cylindrical coordinates for electric and magnetic fields of the form $\psi(r,\phi,z,t)=\psi_n(r)\exp(jm\phi)\exp[j(\omega t-k_z z)]$, where m is an integer denoting angular momentum, n is related to the number of nodes in the radial direction, and k_z is the propagation constant of the mode. The dispersion relation is derived after solving a transcendental equation as obtained by matching boundary conditions [23,32,33]; i.e.,

$$\left[\frac{\varepsilon_3}{k_{T,3}}\frac{J_m'}{J_m}-\frac{\varepsilon_1}{k_{T,1}}\frac{H_m^{(1)\prime}}{H_m^{(1)}}\right]\left[\frac{1}{k_{T,3}}\frac{J_m'}{J_m}-\frac{1}{k_{T,1}}\frac{H_m^{(1)\prime}}{H_m^{(1)}}\right]=m^2\frac{c^2k_z^2}{\omega^2 r_0^2}\left(\frac{1}{k_{T,3}^2}-\frac{1}{k_{T,1}^2}\right)^2, \qquad (4)$$

where $J_m(k_{T,3}r)$ and $H_m^{(1)}(k_{T,1}r)$ represent m-th order Bessel and Hankel functions of the first kind, and

$$k_{T,i} = \sqrt{\left(\frac{\omega}{c}\right)^2 \varepsilon_i - k_z^2} \quad i = 1,3 . \tag{5}$$

The prime above these functions denotes differentiation with respect to their argument. The dispersion relation Eq. (4) differs qualitatively from that of a cylindrical perfect electrical conducting (PEC) waveguide with radius r_0, for which we readily obtain $J_m'(k_{T,3}r_0) = 0$ for transverse electric (TE) and $J_m(k_{T,3}r_0) = 0$ for TM modes [34]. The propagating modes inside the cylindrical hole are calculated by solving for the roots of the dispersion equation, i.e., we numerically determine the (ω, k_z) pairs that satisfy Eq. (4). The procedure involves first a coarse scanning of the (ω, k_z) space to determine the approximate location of the dispersion relation. The solution is then refined using Newton's method.

In what follows, we assume that $\varepsilon_1(\omega)$ takes on the form of Eq. (1) with the collision frequency ω_τ set to zero. This amounts to a lossless plasmonic model. Without loss of generality, we set $\varepsilon_3 = 4$ (e.g., Si_3N_4). For a hole radius $r_0 = 0.36\lambda_p$, where $\lambda_p = 2\pi c/\omega_p$ is the plasma wavelength, the resulting dispersion relations are shown in Fig. 3. We distinguish two types of plasmonic modes: bulk modes, which extend into the metal region and lie above the line defined by $\omega^2 = \omega_p^2 + c^2 k_z^2$; and propagating waveguide modes, which are confined to the hole. The latter exhibit two discrete bands labeled HE_{11} and EH_{11}. The field vector plots of these modes are shown in Fig. 3. These modes with angular momentum $m = 1$ have the proper dipole symmetry to couple to a normally incident plane wave.

The dispersion diagram for the propagating plasmonic modes exhibits three distinct features that have a profound impact on the transmission of incident light through subwavelength cylindrical holes [23]. First, such holes always support propagating modes near the surface plasmon frequency, *regardless of how small the holes are*. Even when material losses are included as part of the plasmonic model, the modes still propagate over several microns when the radius of the holes is much smaller than $\lambda/2n_3$. Second, the fundamental (lowest-frequency) mode has an HE_{11} signature, which enables it to couple to a normally incident plane wave. The HE_{11} mode is located completely below the surface plasmon frequency of the metal. Thus, a cylindrical hole in a plasmonic metal always exhibits a pass-band below the surface plasmon frequency. Third, when the radius of the hole is small, there exists a stop-band for a normally incident plane wave, where the light does not transmit. This stop band occurs when the cut-off at $k_z = 0$ for the EH_{11} mode lies above the surface plasmon frequency. Hence, a single hole or a hole array may behave as a band-pass filter and allow longer wavelengths to pass through while rejecting shorter ones. All of these features are fundamentally different from the behavior of a PEC metal, including a commonly-used modified PEC model where an effective hole radius derived from a skin depth calculation is employed instead [23]. The transmission spectrum of an individual subwavelength hole can be completely explained by the properties of these propagating plasmonic modes. In the case of subwavelength hole arrays, the dispersion relation of a single hole remains very relevant provided that the hole separation is such that the propagating modes inside nearest-neighbor holes do not interact. In fact, this is shown to hold for thickness of separating metal walls as small as 80 nm [23].

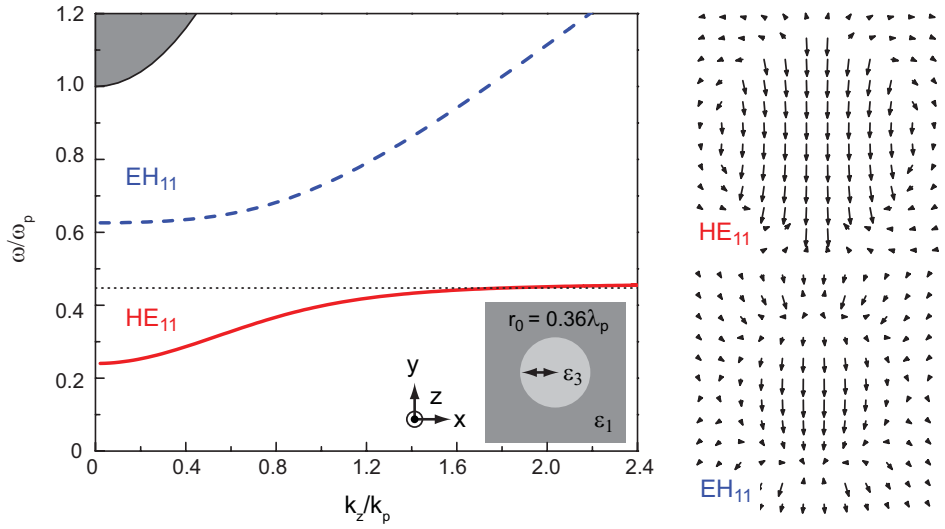

Fig. 3. Dispersion diagram in normalized frequency and wavevector coordinates for a cylindrical hole with radius $0.36\lambda_p$, where λ_p is the plasma wavelength, and the hole is filled with a dielectric ($\varepsilon_3 = 4$). Shown are the two lowest-order waveguide modes with angular momentum $m = 1$ for a lossless plasmonic model. The solid red line corresponds to the dispersion of the HE_{11} mode, while the dashed blue line shows the dispersion of the EH_{11} mode. The side panels show vector plots for the electric fields of the HE_{11} and the EH_{11} mode, respectively.

3.3 Dispersion-based interpretation of extraordinary transmission

We now interpret the transmission spectrum for the subwavelength hole array in Fig. 1 in terms of the dispersion relations for the surface plasmon waves and the propagating plasmonic modes supported by the structure.

Figure 4 (left panel) shows dispersion diagram (ω, k_x) for the surface waves, where ω represents (angular) frequency and k_x denotes the propagation constant parallel to the front and back interfaces of the metallic film. It is obtained using the dispersion model for a single, flat metal-dielectric interface (Section 3.1). We show the lowest-order modes (red and cyan curves) and higher-order modes (gray curves) in the first Brillouin zone of a reduced-zone scheme assuming a square lattice. In this representation, a surface wave will be resonantly excited by normal incident light when the curves intersect the $k_x = 0$ axis. The labeled arrows indicate these locations. For a periodicity $a = 5.43\lambda_p = 750$ nm, the lowest-order (1,0) or (0,1) resonances are excited at $\omega_{(1,0)} = 0.18\omega_p$, the (1,1) resonance occurs at $\omega_{(1,1)} = 0.25\omega_p$, and the (2,0) or (0,2) resonances are located at $\omega_{(2,0)} = 0.34\omega_p$, as determined by Eq. (3). Henceforth, we simplify the notation and refer to these resonances as (1,0), (1,1) and (2,0) SPP resonances, respectively.

Figure 4 (right panel) depicts the dispersion diagram (ω, k_z) of the propagating modes, where k_z denotes the propagation constant along a single subwavelength hole of circular cross-section with radius $r_0 = 120$ nm in a plasmonic metal (blue curves). It is obtained using the method described in Section 3.2.

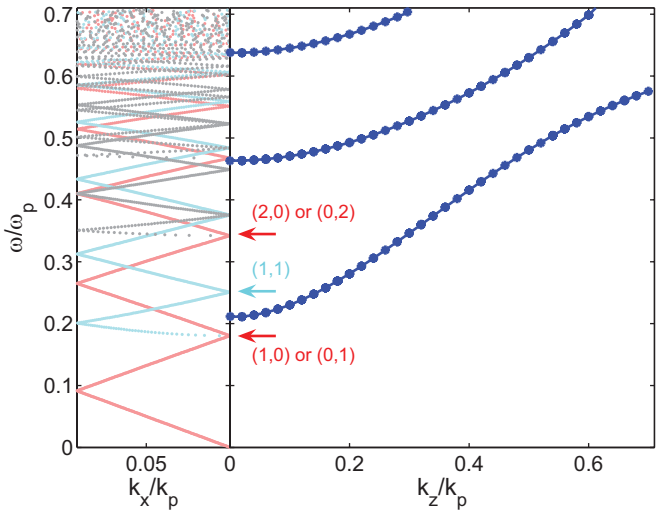

Fig. 4. Dispersion diagram for surface plasmon-polariton modes on a single flat metal-dielectric interface (left panel) and propagating plasmonic modes inside a cylindrical subwavelength hole with circular cross-section (right panel). For the surface waves (red, cyan and gray curves), we assumed a square lattice with periodicity a = 750 nm. For the propagating modes (blue curves), we defined a circular hole with radius r_0 = 120 nm ($r_0 = 0.864\,\lambda_p$). The metal is modeled as a lossless plasmonic material with $\lambda_p = 138\,\text{nm}$ ($\omega_p = 1.37\times10^{16}\,\text{rad/s}$) and the dielectric at the interfaces and inside the hole is air ($\varepsilon_2 = \varepsilon_3 = 1$).

We highlight the following features in the dispersion diagram: $\omega_{HE_{11}} = 0.21\,\omega_p$ is the cutoff frequency for the fundamental HE_{11} mode, $\omega_{EH_{11}} = 0.46\,\omega_p$ is the cutoff frequency for the EH_{11} mode, and $\omega_{sp} = \omega_p/\sqrt{2} = 0.71\,\omega_p$ is the surface plasmon frequency inside the hole.

Next, we overlay the dispersion features on top of the transmission spectrum (Fig. 1). Several SPP resonances occur (solid red and cyan vertical labeled arrows) at 762 nm, 548 nm, and 402 nm. The spectral bandwidth of the propagating HE_{11} mode (solid blue horizontal arrow) ranges from 651 nm (cutoff wavelength) to 309 nm (surface plasmon wavelength inside the hole). This clearly shows that in the wavelength range for which the transmission is shown, both SPP resonances and a propagating HE_{11} mode are present. If only surface waves provide a pathway, as is the case above 651 nm, and normally incident light is coupled into SPP resonances through the momentum added by the hole array, it can give rise to extra-ordinary transmission. This is evidenced by the transmission peaks at 800 nm, near the fundamental (1,0) SPP resonance at 762 nm. This feature is angle and periodicity dependent. The sharp resonance with an asymmetric Fano-interference shape is due to the SPP resonance sitting on a low-transmission (evanescent tunneling inside the holes) background [35-37]. Without material losses, the peaks can reach the 100% transmission level. The double peaks are due to coupling of SPPs on front and back interfaces.

The broad high-transmission plateau below 651 nm arises from the propagating HE_{11} mode inside the holes. Within this range of high transmission, the SPP resonances show up as a dip in the transmission spectrum. In general, when both mechanisms (surface waves and propagating modes) are present simultaneously, their interplay must be studied in order to understand the rich and complex transmission behavior that results. Indeed, the (1,1) and (2,0) SPP resonances reside inside the HE_{11} transmission band. Instead of giving rise to a

transmission peak, they are responsible for the suppression of transmission at 548 nm and 402 nm. (As a side note, the same dips in the spectrum were previously interpreted as Rayleigh-Woods anomalies [14]. In this particular structure, the SPP dispersion relation is very similar to the vacuum dispersion relation. The complex line shapes at 750 and 530 nm in the transmission might be due to the interaction between these two effects [22]. On the other hand, when the SPP and the Rayleigh-Wood anomaly are sufficiently far from each other, both show a dip in the transmission spectra, as seen for example for the two dips in the vicinity of 400 nm. We will show, in Section 4.2, a case where surface plasmon-polariton resonances are well separated from the Rayleigh-Wood anomaly.)

We also note that, in recent studies of metallic systems, localized surface plasmon modes or shape resonances inside the subwavelength holes have been identified as a potential pathway for extraordinary transmission [17-19,22]. These modes are, in fact, a feature of the propagating plasmonic mode near its cutoff wavelength. In order to describe the entire transmission spectrum, in most cases, one really needs to take into account the entire dispersion diagram of the propagating modes and not just their behavior near cutoff. To illustrate this, we refer to the localized waveguide resonance identified in metallic systems featuring subwavelength holes with a rectangular cross-section [21]. For a PEC metal, the resonance is related to a cavity mode at the cut-off frequency of the lowest-order propagating TE_{11} mode. Due to the large impedance mismatch between the hole in a PEC metal and free space, this resonance manifests itself as a single peak in the transmission spectrum surrounded by regions of near-zero transmission (see for example Fig. 2 of Ref. 21). In the case of a plasmonic metal, the lowest-order propagating mode is the HE_{11} mode. It also gives rise to a cavity mode or localized waveguide resonance near its cutoff wavelength. Here, however, the impedance mismatch is smaller and the transmission does not drop abruptly around the highest wavelength peak (see for example Fig. 4 of Ref. 23) and, hence, the entire pass-band of the HE_{11} mode has to be taken into account to explain all the features in the spectrum.

In summary, we find that all salient features in the transmission spectrum (Fig. 1), including dips and peaks, match the highlighted characteristics obtained from the dispersion relations in Fig. 4. Our model not only accounts for the extraordinary transmission peaks at 800 nm due to the (1,0) SPP resonance, but also for the region of background transmission up to 651 nm due to the HE_{11} propagating mode, and for the transmission suppression coinciding with the (1,1) and (2,0) SPP resonances. Hence, the entire extraordinary transmission spectrum can be explained by studying the dispersion of the surface waves and propagating modes supported by the structure.

The typical structure considered in Fig. 1 represents, in fact, only one possible scenario for effects related to extraordinary transmission. In this particular case, the lowest-frequency (1,0) SPP resonance is located below the cut-off frequency of the lowest-order HE_{11} mode, i.e., $\omega_{(1,0)} < \omega_{HE_{11}}$. While this regime is interesting from a theoretical point of view, its usefulness for practical applications merits some discussion. Holes in these designs typically "operate in cutoff", i.e., the cutoff frequency of the propagating plasmonic modes in the hole is above the frequency regime of operation ($\omega < \omega_{HE_{11}}$). Simultaneously, the periodicity of the array is increased to manage losses by bringing the frequency of the (1,0) SPP resonance in the visible or near-infrared range, i.e., away from the surface plasmon frequency of the metal-dielectric interface. Such structures comprise a sparse array (large periodicity) of very small holes and typically feature relatively low transmittance (< 10%), which makes filters based on this approach less attractive. Applications that can benefit from this design should be able to accommodate the lower peak transmittance with a narrow bandwidth that results from the SPP resonance phenomenon. Hence, this regime is more suitable for spectral filtering applications where absolute transmittance is not the main specification.

4 REGIMES OF SUBWAVELENGTH OPERATION

Based on the dispersion analysis for surface waves and propagating modes, we can define several additional regimes of operation for subwavelength apertures. Each regime features subwavelength operation, yet differs in the nature of the pathway(s) that are responsible for transmission. The behavior of subwavelength hole arrays is therefore qualitatively different in each regime, nevertheless the transmission features in each case remain in very good agreement with the dispersion characteristics from surface waves and propagating modes supported by the structures.

We identify four characteristic frequencies in the dispersion analysis of the propagating modes and the surface waves: the cutoff frequency of the HE_{11} mode in the subwavelength holes $\omega_{HE_{11}}$, the surface plasmon frequency in the hole $\omega_{sp,h}$, the frequency of the lowest-order (1,0) SPP resonance $\omega_{(1,0)}$, and the surface plasmon frequency of the flat metal-dielectric interface $\omega_{sp,i}$. The propagating plasmonic HE_{11} mode in the hole is important in the frequency range $\omega_{HE_{11}} < \omega < \omega_{sp,h}$, whereas the SPP resonances appear in the frequency range $\omega_{(1,0)} < \omega < \omega_{sp,i}$. We define the regimes of operation for subwavelength aperture arrays based on the respective order of these characteristic frequencies. This order establishes the location and potential spectral overlap of the different mechanisms or pathways. It profoundly impacts the transmission spectrum, as evidenced in the "Ebbesen" regime (Section 3.3) where the order is $\omega_{(1,0)} < \omega_{HE_{11}} < \omega_{sp,h} = \omega_{sp,i}$.

In what follows, we assume again, for simplicity and without loss of generality, a circular hole with radius $r_0 = 0.36\lambda_p$ and a square lattice with periodicity a = 180 nm. The metal is described by the plasmonic model Eq. (1) with plasma frequency $\omega_p = 1.37\times10^{16}$ rad/s and collision frequency $\omega_\tau = 7.29\times10^{13}$ rad/s. When a lossless plasmonic model is used, the collision frequency ω_τ is set to zero. Using a combination of dispersion analysis and 3D FDTD simulations, we investigate the transmission of subwavelength hole array structures for each of the different regimes and identify which modes play the dominant role in the transport properties for incident light.

4.1 Regime 1: $\omega_{HE11} < \omega_{sp,h} < \omega_{(1,0)}$

In the structure of Fig. 1, the SPP resonances occur at discrete locations in the frequency range between $\omega_{(1,0)} = 0.18\omega_p$ and $\omega_{sp} = \omega_p/\sqrt{2}$, while the hole supports propagating modes in the entire range between $\omega_{HE_{11}} = 0.21\omega_p$ and $\omega_{sp} = \omega_p/\sqrt{2}$. Hence, the two frequency ranges largely overlap. By placing a dielectric inside the hole, however, it is possible to shift the range of propagating modes to lower frequencies, thereby avoiding spectral overlap with the SPP resonance range. In this regime, we have $\omega_{HE_{11}} < \omega_{sp,h} < \omega_{(1,0)}$ and each pathway should separately lead to large transmission and no destructive interference (transmission suppression) should arise. We recently identified this regime of operation for subwavelength holes and found that the presence of a plasmonic HE_{11} mode alone, indeed, leads to near-complete optical transmission [23]. To the best of our knowledge, this regime has not been probed yet experimentally.

Figure 5 shows the dispersion diagram (ω, k_x) for the surface waves (left panel; red, cyan and gray curves) and the dispersion diagram (ω, k_z) for the propagating modes (right panel; blue and magenta curves). For periodicity $a = 1.30\lambda_p$, the lowest-order (1,0) SPP resonance

is excited at $\omega_{(1,0)} = 0.56\,\omega_p$ (left panel). The dispersion diagram for the propagating modes in the hole, on the other hand, features three discrete bands (right panel). The first band (lower solid blue curve), located between $\omega_{HE_{11}} = 0.24\,\omega_p$ and $\omega_{sp} = \omega_p / \sqrt{5}$, corresponds to the lowest-order HE_{11} mode. A second band (upper solid blue curve) features frequencies larger than $\omega_{EH_{11}} = 0.63\,\omega_p$ and depicts the dispersion of the higher-order EH_{11} mode. Both modes have angular momentum $m = 1$ and couple to normally incident light. A third mode (solid magenta curve) is located between $\omega_{m=3} = 0.38\,\omega_p$ and $\omega_{sp} = \omega_p / \sqrt{5}$, and has angular momentum $m = 3$. In a single hole, the $m = 3$ mode does not have the right dipole symmetry to couple to a plane wave. As we will show below, the square lattice breaks the continuous rotational symmetry of a single hole and allows the plane wave to actually couple to this mode as well. Between the discrete bands, from $\omega_{sp} = \omega_p / \sqrt{5}$ to $\omega_{EH_{11}} = 0.63\,\omega_p$, is a stop-band where no propagating modes exist in a subwavelength hole with radius $r_0 = 0.36\,\lambda_p$.

Figure 6 shows the transmission spectrum at normal incidence for a subwavelength hole array operating in this regime. The dominant feature is a high-transmission pass-band from 309 nm to 573 nm. The pass-band features a bandwidth (blue horizontal arrow) that agrees perfectly with the dispersion of the HE_{11} propagating mode (lower solid blue curve in the right panel of Fig. 5). We note that, in contrast to the dominant feature in the "Ebbesen" regime (Fig. 1), the pass-band is due to the propagating mode inside the subwavelength hole. Hence, it is largely independent of incidence angle or periodicity of the array. It is also the longest-wavelength feature in the transmission spectrum of the structure, since $\omega_{HE_{11}} = 0.24\,\omega_p$ is smaller than $\omega_{(1,0)} = 0.56\,\omega_p$. A second distinct feature in the transmission spectrum is the low-transmission region between 220 nm and 309 nm. This is the stop-band between the propagating HE_{11} and EH_{11} modes and once again the range agrees very well with the dispersion analysis (Fig. 5 right panel). A third spectral feature is a sharp, narrow 100% transmission peak in the stop-band at 245 nm (vertical red arrow). This wavelength corresponds with the location of the (1,0) SPP resonance in the dispersion analysis (Fig. 5 left panel). Since the SPP resonance is located in the stop-band between propagating plasmonic modes in the hole, it shows up as a resonant transmission peak.

Finally, notice the sharp asymmetric peaks between 309 nm and 413 nm. This range agrees with spectral bandwidth of the plasmonic propagating mode with angular momentum $m = 3$ (magenta curve in right panel of Fig. 5). The peaks result from Fano interference between multiple pathways. In this case, the pathways are formed by the fundamental HE_{11} mode (blue horizontal arrow), which couples very efficiently to the incident light, and the higher-order $m = 3$ mode (magenta horizontal arrow). In a single hole, this mode does not have the proper (dipole) symmetry to couple to an incident plane wave. The presence of a square lattice, however, may result in coupling of light into this mode, since 3-fold rotation is no longer the symmetry of the structure. To verify this interpretation, we plot the H_z-component of the magnetic field as an inset for the Fano interference-peak at 408 nm. The field exhibits the six nodes that are characteristics of modes with $m = 3$ symmetry. The frequency of this mode lies outside the spectral band of the $m = 3$ mode for a single subwavelength hole (magenta horizontal arrow). Since the symmetry-breaking arises from the lattice and, hence, the coupling between the holes, we speculate that the coupling between the holes may also lead to a shift in the spectral band in the hole array. These interference peaks have not yet been reported experimentally. Indeed, we have verified that the features in the band due to the higher-order $m = 3$ propagating mode, as well as the (1,0) surface resonance peak, all vanish when losses are included in the metal model (Fig. 7). In what follows, we proceed with a lossy plasmonic model.

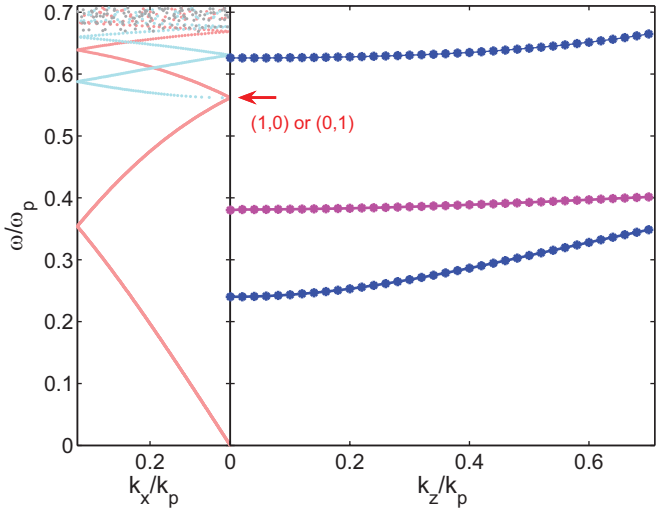

Fig. 5. Dispersion diagram for the surface plasmon-polariton modes (red, cyan and gray curves) and the propagating plasmonic modes in Regime 1. Shown are the HE_{11} and EH_{11} modes with angular momentum m = 1 (blue curves) and the first propagating mode with m = 3 (magenta curve). The metal is modeled as a lossless plasmonic material with $\lambda_p = 138\,\text{nm}$ ($\omega_p = 1.37\times10^{16}\,\text{rad/s}$), the film is surrounded by air ($\varepsilon_2 = 1$) and the hole is filled with a dielectric ($\varepsilon_3 = 4$).

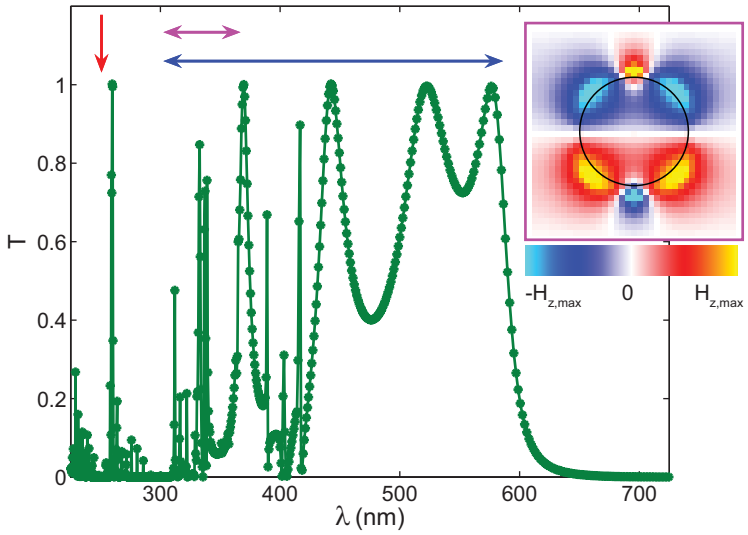

Fig. 6. Normal-incidence transmission spectrum of a 50-nm radius ($r_0 = 0.36\lambda_p$) cylindrical hole array with 180-nm period in a 250-nm thick metal film. The hole, surround, and metal properties are the same as in Fig. 5. The surface resonance is indicated by the red vertical arrow. The blue and magenta horizontal arrows show the range of the lowest-order propagating modes in the hole with m = 1 and m = 3, respectively. Inset shows the H_z-component of the magnetic field for the Fano-interference peak at 408 nm.

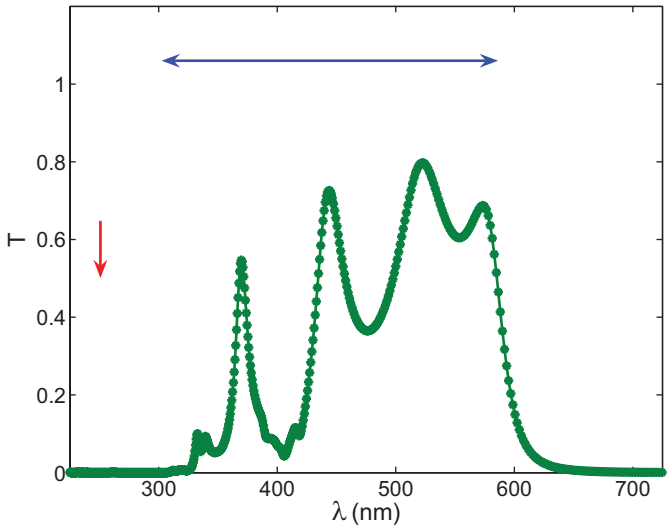

Fig. 7. Normal-incidence transmission spectrum of a 50-nm radius ($r_0 = 0.36\lambda_p$) cylindrical hole array with 180-nm period in a 250-nm thick metal film. The metal is modeled as a lossy plasmonic material with $\lambda_p = 138\,\text{nm}$ ($\omega_p = 1.37\times10^{16}$ rad/s) and $\omega_\tau = 7.29\times10^{13}$ rad/s . The surface resonance is indicated by the red vertical arrow. The blue horizontal arrows show the range of the lowest-order propagating modes in the hole with m = 1.

Hole array designs based on this approach typically feature a high packing density and exhibit diffraction-less behavior. These structures have a high-transmission pass-band with a finite bandwidth that is non-resonant and that can be tailored at both the low and high-frequency ends. This regime is ideal for applications that require a broad-band filter such as solar cells, color imaging, polarimetry, or color displays.

4.2 Regime 2: $\omega_{HE11} < \omega_{(1,0)} < \omega_{sp,h}$

Another class of subwavelength hole array designs consists of selecting the periodicity of the array and the hole size such that the presence of the lowest-order (1,0) SPP resonance falls within the spectral range of the propagating HE_{11} mode. In this regime $\omega_{HE_{11}} < \omega_{(1,0)} < \omega_{sp,h}$ and both pathways are present simultaneously in the regime of operation and play a crucial role in the transmission behavior.

Figure 8 shows the dispersion diagram (ω, k_x) for the surface waves (left panel; red, cyan and gray curves) and the dispersion diagram (ω, k_z) for the propagating modes (right panel; blue curve). For a lattice constant $a = 1.30\lambda_p$, the lowest-order (1,0) SPP resonance is excited at $\omega_{(1,0)} = 0.56\,\omega_p$ (left panel). The dispersion diagram for the propagating modes in the hole (right panel), on the other hand, features the lowest-order HE_{11} mode ($m = 1$) that exists between $\omega_{HE_{11}} = 0.46\,\omega_p$ and $\omega = \omega_p / \sqrt{2}$. Hence, the (1,0) SPP resonance is located within the spectral band of the propagating HE_{11} mode.

Figure 9 shows the transmission spectrum for this design obtained with 3D FDTD calculations. The agreement with the dispersion characteristics is indicated, as before, by the blue horizontal arrow and the vertical red arrow.

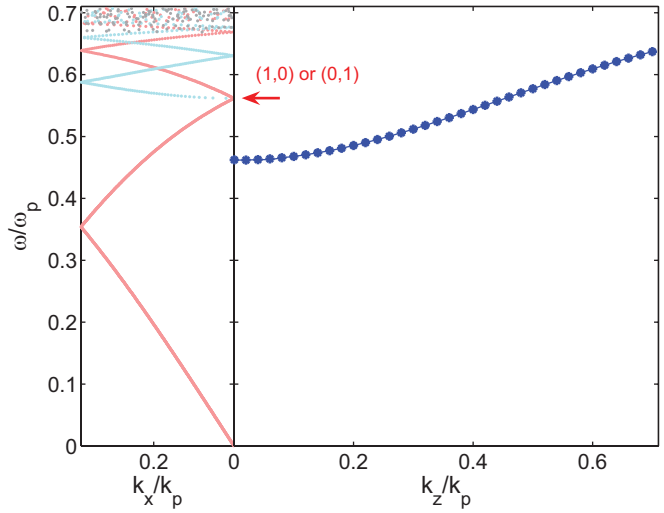

Fig. 8. Dispersion diagram for the surface plasmon-polariton modes (red, cyan and gray curves) and the propagating plasmonic modes (blue curves) in Regime 2. The metal is modeled as a lossy plasmonic material with $\lambda_p = 138\,\text{nm}$ ($\omega_p = 1.37\times10^{16}$ rad/s) and $\omega_\tau = 7.29\times10^{13}$ rad/s. The film is surrounded by air ($\varepsilon_2 = 1$) and the hole is filled with air ($\varepsilon_3 = 1$).

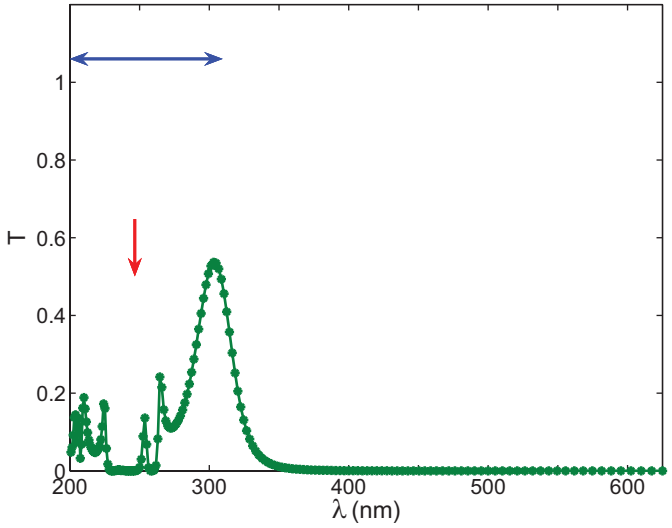

Fig. 9. Normal-incidence transmission spectrum of a 50-nm radius ($r_0 = 0.36\lambda_p$) cylindrical hole array with 180-nm period in a 250-nm thick metal film. The hole, surround, and metal properties are the same as in Fig. 8. The surface resonance is indicated by the red vertical arrow. The blue horizontal arrow shows the range of the propagating mode in the hole.

Due to the simultaneous presence of two transmission pathways, we observe two very striking effects. First, the spectrum features a high-transmission pass-band between 250 nm and 350 nm. This feature is primarily due to the excitation of propagating modes inside the holes. Even though the interaction between propagating modes and surface resonances leads to a shift of the high-transmission window to the longer wavelength range, the oscillation due to Fabry-Perot effects inside the hole is preserved. Second, the transmission is completely suppressed from 225 nm to 250 nm. This feature arises from Fano interference [38] between two transmission pathways, formed by propagating modes in the holes and surface resonances on the interfaces.

The high-transmission peak at 300 nm, which coincides with the cutoff frequency of the propagating HE_{11} mode ($k_z = 0$), can be interpreted as a localized waveguide resonance [21]. It is evident from the transmission spectrum, however, that a description in terms of a localized waveguide resonance alone is not complete. Instead, the full pass-band of the plasmonic mode has to be taken into account (This was also evidenced in Figs. 6 and 7, where only the Fabry-Perot wavelength peaks correspond to the localized waveguide resonances, but there are regions of high transmission in between as well).

4.3 Regime 3: $\omega_{(1,0)} < \omega_{sp,i} < \omega_{HE11}$

It is possible, in general, to independently engineer the hole and the interface properties in the aperture systems discussed in this paper. For example, rather than placing a dielectric inside the hole (Regime 1), we can instead apply a thin dielectric coating to the interfaces of the film. The presence of a coating shifts all the SPP resonances to lower frequencies so that they do not overlap with the range in which the propagating modes occur. In this case $\omega_{(1,0)} < \omega_{sp,i} < \omega_{HE_{11}}$ and the structure operates in a regime where each pathway can separately lead to large transmission without destructive interference (transmission suppression). This regime looks similar to Regime 1. In comparison, however, the frequency-order of pathways is reversed in this regime.

The design of such a structure, specifically, is based on the idea that one can engineer the cutoff frequency of the hole $\omega_{HE_{11}}$ to lie above the surface plasmon frequency of the interfaces $\omega_{sp,i}$. For example, the hole radius ($r_0 = 0.36\lambda_p$) and dielectric inside the hole ($\varepsilon_3 = 1$) determine the cutoff frequency of the propagating HE_{11} mode inside the subwavelength hole at $\omega_{HE_{11}} = 0.46\omega_p$. The thin dielectric coating enforces a limiting frequency for the surface waves supported by the interfaces. For large k_x-values, the surface waves are highly confined to the interface and they see only the coating. Hence, their limiting frequency value is the surface plasmon frequency of the metal-coating interface $\omega_{sp} = \omega_p / \sqrt{1+\varepsilon_c} < \omega_{HE_{11}}$ (irrespective of the properties of the surrounding medium), where ε_c is the dielectric constant of the thin coating. In this case, it is no longer sufficient to employ the dispersion relations for a single metal-dielectric interface [Eqs. (2) and (3)] to estimate the dispersion diagram. Rather, one has to calculate the dispersion of the modes supported by a three-layer system, consisting of a semi-infinite dielectric superstrate with dielectric constant $\varepsilon_2 > 0$, a thin dielectric coating with dielectric constant $\varepsilon_c > 0$ and thickness h_c, and a semi-infinite metal substrate with dielectric function $\varepsilon_1(\omega) < 0$. The resulting dispersion equation, which has to be solved, is given by

$$\left(\frac{k_{2z}}{\varepsilon_2} + \frac{k_{1z}}{\varepsilon_1}\right) = j\left(\frac{\varepsilon_c}{k_{cz}}\frac{k_{2z}k_{1z}}{\varepsilon_1\varepsilon_2} + \frac{k_{cz}}{\varepsilon_c}\right)\tan\left(k_{cz}h_c\right), \tag{6}$$

where $k_{iz} = \sqrt{\varepsilon_i (\omega/c)^2 - k_x^2}$ is the wavevector component perpendicular to the surface and k_x is parallel to the surface. Solving this transcendental equation leads to the dispersion diagram for modes supported by a dielectric coated interface. The lowest-order mode that results is a surface wave.

Figure 10 shows the dispersion diagram (ω, k_x) for the surface waves supported by the coated surface (left panel; red, cyan and gray curves) and the dispersion (ω, k_z) of the propagating mode inside the hole (right panel; blue curve). The lowest-order (1,0) SPP resonance is excited at $\omega_{(1,0)} = 0.37\,\omega_p$ (left panel) and all higher-order surface resonance are located below $\omega_{sp} = \omega_p / \sqrt{5}$. The dispersion diagram for the propagating HE_{11} mode in the hole (right panel), on the other hand, starts at $\omega_{HE_{11}} = 0.46\,\omega_p$. Therefore, both mechanisms are spectrally separated and do not interact.

Figure 11 features the transmission spectrum at normal incidence obtained using 3D FDTD calculations. The arrows indicate the features derived from the dispersion diagram. Specifically, the (1,0) SPP resonance at 368 nm due to the surface modes (red vertical arrow), agrees very well with the transmission peak at 400 nm. The transmission regime between 200 nm and 300 nm matches perfectly with the pass-band due to the propagating HE_{11} mode (blue horizontal arrow). These results identify a new regime of operation that until now has not been analyzed theoretically and has not been explored experimentally either. Nevertheless, it features a clean separation of the surface plasmon and propagating plasmonic modes by design and therefore should be useful in establishing the transmission properties that are unique to each of the types of modes.

5 DISCUSSION AND SUMMARY

We studied the interaction of different mechanisms or pathways by which extraordinary transmission through subwavelength and nanoscale aperture arrays can arise in metallic systems. We provide a complete physical picture that incorporates both propagating plasmonic and surface plasmon modes. Our study incorporates all previously reported mechanisms, e.g., surface-plasmon resonances, localized plasmon resonances and propagating plasmonic modes, and unifies them in a comprehensive dispersion-based framework. We re-visited the regime explored by Ebbesen *et al.* [12] and showed that our approach explains all the salient features in the transmission spectrum, including the ones ascribed to surface waves. We provided evidence that shape resonances or localized surface plasmons are, in fact, due to the behavior of propagating plasmonic modes inside the holes near their cutoff frequency. We identified four characteristic frequencies: the cutoff frequency of the HE_{11} mode in the holes, the surface plasmon frequency in the hole, the frequency of the lowest-order SPP resonance, and the surface plasmon frequency of the interface. We defined several regimes of operation for subwavelength aperture arrays, based on the respective order of the characteristic frequencies. We designed subwavelength hole arrays to probe these regimes, including the "Ebbesen" regime [14], a regime we previously reported in Refs. 23 and 24, and a newly identified regime. In each case, the dispersion analysis explains the details of the transmission spectrum. Finally, we showed that the transmission behavior is qualitatively different depending on the number of transmission pathways present in the regime of operation. If only one mechanism is present, it can give rise to extraordinary transmission. When both mechanisms are present simultaneously, their interplay must be studied in order to understand the rich and complex transmission behavior that results. The same set of interference effects and mechanisms can be found in other resonant systems as well.

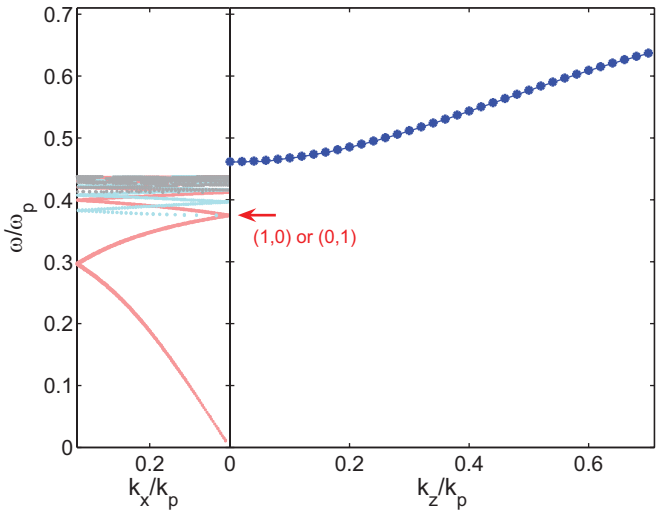

Fig. 10. Dispersion diagram for propagating plasmonic (blue curves) and surface plasmon-polariton modes (red, cyan and gray curves) in Regime 3. The metal is modeled as a lossy plasmonic material with $\lambda_p = 138\,\text{nm}$ ($\omega_p = 1.37\times10^{16}$ rad/s) and $\omega_\tau = 7.29\times10^{13}$ rad/s . The hole is filled with air ($\varepsilon_3 = 1$), the horizontal metal surfaces are coated with the thin dielectric layer ($\varepsilon_c = 4$, $h_c = 20\,\text{nm}$) and the film is surrounded by air ($\varepsilon_2 = 1$).

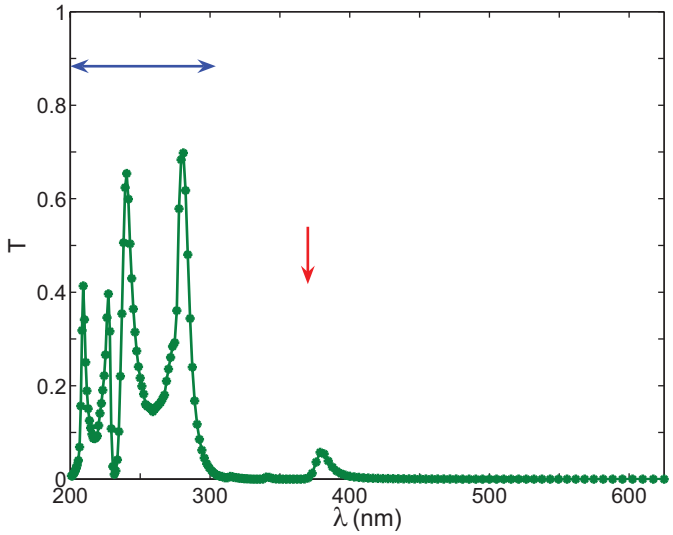

Fig. 11. Normal-incidence transmission spectrum of a 50-nm radius ($r_0 = 0.36\lambda_p$) cylindrical hole array with 180-nm period in a 250-nm thick metal film. The hole, coating, surround, and metal properties are the same as in Fig. 10. The surface resonance is indicated by the red vertical arrow. The blue horizontal arrow shows the range of the propagating mode in the hole.

For example, we recently reported at mid-infrared wavelengths that phonon-polaritonic thin films with a periodic array of subwavelength holes allow near-complete transmission in the polariton gap where a homogeneous film completely suppresses transmission and we observed similar interference effects [37].

Acknowledgments

This work was supported in part by the Stanford Global Climate and Energy Project (GCEP), and by the NSF-NIRT Program (Grant No. ECS-0507301). The computation was performed with support from the NSF-LRAC program.

References

[1] S. Blair and A. Nahata, "Focus issue: Extraordinary light transmission through sub-wavelength structured surfaces - Introduction," *Opt. Exp.* **12**(16), 3618-3618 (2004) [doi:10.1364/OPEX.12.003618].

[2] C. Genet and T. W. Ebbesen, "Light in tiny holes," *Nature* **445**(7123), 39-46 (2007) [doi:10.1038/nature05350].

[3] J. A. Porto, F. J. Garcia-Vidal, and J. B. Pendry, "Transmission resonances on metallic gratings with very narrow slits," *Phys. Rev. Lett.* **83**(14), 2845-2848 (1999) [doi:10.1103/PhysRevLett.83.2845].

[4] F. I. Baida and D. Van Labeke, "Three-dimensional structures for enhanced transmission through a metallic film: Annular aperture arrays," *Phys. Rev. B* **67**(15), 155314 (2003) [doi:10.1103/PhysRevB.67.155314].

[5] E. Popov, M. Neviere, S. Enoch, and R. Reinisch, "Theory of light transmission through subwavelength periodic hole arrays," *Phys. Rev. B* **62**(23), 16100-16108 (2000) [doi:10.1103/PhysRevB.62.16100].

[6] P. Lalanne, J. P. Hogonin, S. Astilean, M. Palamaru, and K. D. Moller, "One-mode model and Airy-like formulae for one-dimensional metallic gratings," *J. Opt. A: Pure Appl. Opt.* **2**, 48-51 (2000) [doi:10.1088/1464-4258/2/1/309].

[7] S. Astilean, P. Lalanne, and M. Palamaru, "Light transmission through metallic channels much smaller than the wavelength," *Opt. Commun.* **175**(4), 265-273 (2000) [doi:10.1016/S0030-4018(00)00462-4].

[8] Y. Takakura, "Optical resonance in a narrow slit in a thick metallic screen," *Phys. Rev. Lett.* **86**(24), 5601-5603 (2001) [doi:10.1103/PhysRevLett.86.5601].

[9] Q. Cao and P. Lalanne, "Negative role of surface plasmons in the transmission of metallic gratings with very narrow slits," *Phys. Rev. Lett.* **88**(5), 057403 (2002) [doi:10.1103/PhysRevLett.88.057403].

[10] W. L. Barnes, W. A. Murray, J. Dintinger, E. Devaux, and T. W. Ebbesen, "Surface plasmon polaritons and their role in the enhanced transmission of light through periodic arrays of subwavelength holes in a metal film.," *Phys. Rev. Lett.* **92**(10), 107401 (2004) [doi:10.1103/PhysRevLett.92.107401].

[11] W. L. Barnes, A. Dereux, and T. W. Ebbesen, "Surface plasmon subwavelength optics," *Nature* **424**(6950), 824-830 (2003) [doi:10.1038/nature01937].

[12] T. W. Ebbesen, H. J. Lezec, H. F. Ghaemi, T. Thio, and P. A. Wolff, "Extraordinary optical transmission through sub-wavelength hole arrays," *Nature* **391**(6668), 667-669 (1998) [doi:10.1038/35570].

[13] A. Krishnan, T. Thio, T. J. Kima, H. J. Lezec, T. W. Ebbesen, P. A. Wolff, J. Pendry, L. Martin-Moreno, and F. J. Garcia-Vidal, "Evanescently coupled resonance in surface plasmon enhanced transmission," *Opt. Commun.* **200**(1), 1-7 (2001) [doi:10.1016/S0030-4018(01)01558-9].

[14] L. Martin-Moreno, F. J. Garcia-Vidal, H. J. Lezec, K. M. Pellerin, T. Thio, J. B. Pendry, and T. W. Ebbesen, "Theory of extraordinary optical transmission through

subwavelength hole arrays," *Phys. Rev. Lett.* **86**(6), 1114-1117 (2001) [doi:10.1103/PhysRevLett.86.1114].

[15] J. B. Pendry, L. Martin-Moreno, and F. J. Garcia-Vidal, "Mimicking surface plasmons with structured surfaces," *Science* **305**(5685), 847-848 (2004) [doi:10.1126/science.1098999].

[16] H. J. Lezec and T. Thio, "Diffracted evanescent wave model for enhanced and suppressed optical transmission through subwavelength hole arrays," *Opt. Exp.* **12**(16), 3629-3651 (2004) [doi:10.1364/OPEX.12.003629].

[17] K. J. K. Koerkamp, S. Enoch, F. B. Segerink, N. F. van Hulst, and L. Kuipers, "Strong influence of hole shape on extraordinary transmission through periodic arrays of subwavelength holes," *Phys. Rev. Lett.* **92**(18), 183901 (2004) [doi:10.1103/PhysRevLett.92.183901].

[18] A. Degiron and T. W. Ebbesen, "The role of localized surface plasmon modes in the enhanced transmission of periodic subwavelength apertures," *J. Opt. A: Pure Appl. Opt.* **7**(2), S90-S96 (2005) [doi:10.1088/1464-4258/7/2/012].

[19] K. L. van der Molen, K. J. Klein Koerkamp, S. Enoch, F. B. Segerink, N. F. van Hulst, and L. Kuipers, "Role of shape and localized resonances in extraordinary transmission through periodic arrays of subwavelength holes: Experiment and theory," *Phys. Rev. B* **72**(4), 183901 (2005) [doi:10.1103/PhysRevLett.92.183901].

[20] R. Gordon, A. G. Brolo, A. McKinnon, A. Rajora, B. Leathem, and K. L. Kavanagh, "Strong polarization in the optical transmission through elliptical nanohole arrays," *Phys. Rev. Lett.* **92**(3), 037401 (2004) [doi:10.1103/PhysRevLett.92.037401].

[21] Z. C. Ruan and M. Qiu, "Enhanced transmission through periodic arrays of subwavelength holes: The role of localized waveguide resonances," *Phys. Rev. Lett.* **96**(23), 233901 (2006) [doi:10.1103/PhysRevLett.96.233901].

[22] C. Huang, Q. Wang, and Y. Zhu, "Dual effect of surface plasmons in light transmission through perforated metal films," *Phys. Rev. B* **75**(24), 245421 (2007) [doi:10.1103/PhysRevB.75.245421].

[23] H. Shin, P. B. Catrysse, and S. Fan, "Effect of the plasmonic dispersion relation on the transmission properties of subwavelength cylindrical holes," *Phys. Rev. B* **72**(8), 085436 (2005) [doi:10.1103/PhysRevB.72.085436].

[24] P. B. Catrysse, H. Shin, and S. H. Fan, "Propagating modes in subwavelength cylindrical holes," *J. Vac. Sci. Technol. B* **23**(6), 2675-2678 (2005) [doi:10.1116/1.2130344].

[25] C. F. Bohren and D. R. Huffman, *Absorption and Scattering of Light by Small Particles*, Wiley, New York (1983).

[26] M. A. Ordal, L. L. Long, R. J. Bell, S. E. Bell, R. R. Bell, R. W. Alexander, Jr., and C. A. Ward, "Optical properties of the metals Al, Co, Cu, Au, Fe, Pb, Ni, Pd, Pt, Ag, Ti and W in the infrared and far infrared," *Appl. Opt.* **22**(7), 1099-1119 (1983).

[27] M. A. Ordal, R. J. Bell, R. W. Alexander, Jr., L. L. Long, and M. R. Querry, "Optical properties of fourteen metals in the infrared and far infrared: Al, Co, Cu, Au, Fe, Pb, Mo, Ni, Pd, Pt, Ag, Ti, V, and W," *Appl. Opt.* **24**(24), 4493-4499 (1985).

[28] A. D. Rakic, A. B. Djurisic, J. M. Elazar, and M. L. Majewski, "Optical properties of metallic films for vertical-cavity optoelectronic devices.," *Appl. Opt.* **37**(22), 5271-5283 (1998).

[29] A. Taflove and S. C. Hagness, *Computational Electrodynamics: the Finite-Difference Time-Domain Method*, 2nd / ed, Artech House, Boston (2000).

[30] J. P. Berenger, "A perfectly matched layer for the absorption of electromagnetic-waves," *J. Comput. Phys.* **114**(2), 185-200 (1994) [doi:10.1006/jcph.1994.1159].

[31] S. H. Fan and J. D. Joannopoulos, "Analysis of guided resonances in photonic crystal slabs," *Phys. Rev. B* **65**(23), 235112 (2002) [doi:10.1103/PhysRevB.65.235112].

[32] L. Novotny and C. Hafner, "Light propagation in a cylindrical waveguide with a complex, metallic, dielectric function," *Phys. Rev. E* **50**(5), 4094-4106 (1994) [doi:10.1103/PhysRevE.50.4094].
[33] C. A. Pfeiffer, E. N. Economou, and K. L. Ngai, "Surface polaritons in a circularly cylindrical interface: surface plasmons," *Phys. Rev. B* **10**(8), 3038-3051 (1974) [doi:10.1103/PhysRevB.10.3038].
[34] D. M. Pozar, *Microwave Engineering*, 2nd ed, John Wiley & Sons, New York (1997).
[35] M. Sarrazin, J. P. Vigneron, and J. M. Vigoureux, "Role of Wood anomalies in optical properties of thin metallic films with a bidimensional array of subwavelength holes," *Phys. Rev. B* **67**(8), 85415 (2003) [doi:10.1103/PhysRevB.67.085415].
[36] C. Genet, M. P. van Exter, and J. P. Woerdman, "Fano-type interpretation of red shifts and red tails in hole array transmission spectra," *Opt. Commun.* **225**(4-6), 331-336 (2003) [doi:10.1016/j.optcom.2003.07.037].
[37] P. B. Catrysse and S. H. Fan, "Near-complete transmission through subwavelength hole arrays in phonon-polaritonic thin films," *Phys. Rev. B* **75**(7), 075422 (2007) [doi:10.1103/PhysRevB.75.075422].
[38] U. Fano, "Effects of configuration interaction on intensities and phase shifts," *Phys. Rev.* **124**(6), 1866-1878 (1961) [doi:10.1103/PhysRev.124.1866].

Peter B. Catrysse is an engineering research associate in the Edward L. Ginzton Laboratory at Stanford University, CA (USA). He received his Ph.D. degree in electrical engineering from Stanford University in 2003. He is the author of more than 40 refereed articles and he has given more than 25 invited and contributed talks. He also holds 4 U.S. patents. His current research interests include nanophotonics, plasmonics, metamaterials, optical sensing, and CMOS sensors. Dr. Catrysse was the recipient of the 1996 Brussels Hoover Fellowship of the Belgian American Educational Foundation, Inc. and a Fund for Scientific Research – Flanders (Belgium) Fellowship in 1998. He is a member of OSA, IEEE, MRS, and SPIE.

Shanhui Fan is an associate professor of electrical engineering at the Stanford University. He received his Ph.D. in 1997 in theoretical condensed matter physics from the Massachusetts Institute of Technology (MIT), and was a research scientist at the Research Laboratory of Electronics at MIT prior to his appointment at Stanford. His research interests are in computational and theoretical studies of solid state and photonic structures and devices, especially photonic crystals, micro-cavities, and nanophotonic circuits and elements. He has published over 140 refereed journal articles, has given over 100 invited talks, and was granted 28 U.S. patents. Prof. Fan received a National Science Foundation Career Award (2002), a David and Lucile Packard Fellowship in Science and Engineering (2003), the National Academy of Sciences Award for Initiative in Research (2007), and the Adolph Lomb Medal from the Optical Society of America (2007). Dr. Fan is Fellow of OSA, a senior member of IEEE, and a member of APS and SPIE.